

# NJC

Accepted Manuscript



This article can be cited before page numbers have been issued, to do this please use: S. Banerjee, P. Brandao, A. Bauza, A. Frontera, M. Barcelo-Oliver, A. Panja and A. Saha, *New J. Chem.*, 2017, DOI: 10.1039/C7NJ02280H.



This is an Accepted Manuscript, which has been through the Royal Society of Chemistry peer review process and has been accepted for publication.

Accepted Manuscripts are published online shortly after acceptance, before technical editing, formatting and proof reading. Using this free service, authors can make their results available to the community, in citable form, before we publish the edited article. We will replace this Accepted Manuscript with the edited and formatted Advance Article as soon as it is available.

You can find more information about Accepted Manuscripts in the [author guidelines](#).

Please note that technical editing may introduce minor changes to the text and/or graphics, which may alter content. The journal's standard [Terms & Conditions](#) and the ethical guidelines, outlined in our [author and reviewer resource centre](#), still apply. In no event shall the Royal Society of Chemistry be held responsible for any errors or omissions in this Accepted Manuscript or any consequences arising from the use of any information it contains.

# Nuclearity versus oxidation state in catalytic efficiency of Mn<sup>II/III</sup> azo Schiff base complexes: Computational study on supramolecular interactions and phenoxazinone synthase like activity

Saikat Banerjee,<sup>a</sup> Paula Brandão,<sup>b</sup> Antonio Bauzá,<sup>c</sup> Antonio Frontera,<sup>\*c</sup> Miquel Barceló-Oliver<sup>c</sup>, Anangamohan Panja,<sup>d</sup> and Amrita Saha,<sup>\*a</sup>

<sup>a</sup> Department of Chemistry, Jadavpur University, Kolkata- 700032, India.

E-mail: amritasahachemju@gmail.com; asaha@chemistry.jdvu.ac.in; Tel. +91-33-2457294.

<sup>b</sup> Departamento de Química, CICECO, Universidade de Aveiro, 3810-193 Aveiro, Portugal.

<sup>c</sup> Departament de Química, Universitat de les Illes Balears, Crta. De Valldemossa km 7.5, 07122 Palma (Balears), Spain.

E-mail: toni.frontera@uib.es.

<sup>d</sup> Postgraduate Department of Chemistry, Panskura Banamali College, Panskura RS, WB 721152, India.

## Abstract

A novel mononuclear Mn(III) complex, [Mn<sup>III</sup>(L<sup>1</sup>)Cl(H<sub>2</sub>O)].H<sub>2</sub>O (**1**), and a tetranuclear Zn(II)-Mn(II) complex, [{Zn<sup>II</sup><sub>2</sub>(L<sup>2</sup>)<sub>2</sub>Cl<sub>2</sub>}Mn<sup>II</sup><sub>2</sub>(μ<sub>1,1</sub>-N<sub>3</sub>)<sub>2</sub>(H<sub>2</sub>O)<sub>2</sub>].2H<sub>2</sub>O (**2**), have been synthesized involving azo Schiff base ligands viz. H<sub>2</sub>L<sup>1</sup> = (E)-6,6'-((1E,1'E)-(ethane-1,2-diylbis(azanylylidene))bis(methanylylidene))bis(2-methoxy-4-((E)-p-tolyldiazenyl)phenol) and H<sub>2</sub>L<sup>2</sup> = (E)-6,6'-((1E,1'E)-((2,2-dimethylpropane-1,3-diyl)bis(azanylylidene))bis(methanylylidene))bis(2-methoxy-4-((E)-p-tolyldiazenyl)phenol), respectively. The solid-state structures were determined by single crystal X-ray crystallography. In complex **1**, the Mn(III) centre adopts an almost perfect octahedral geometry, while in complex **2** the Mn(II) centre residing in outer core of the ligand adopts a distorted pentagonal bipyramidal geometry. In complex **1**, chloride ion simply acts as a terminal ligand. While, in complex **2** azide ions bind the metal centres in an end-on bridging fashion to produce a tetranuclear complex. Phenoxazinone synthase like activity of both complexes has been examined and a detail structure-property correlation has been performed. Whereas, the mononuclear complex **1** exhibits significant phenoxazinone activity, complex **2** is almost inactive, although in both complexes

labile sites are available at manganese centres for substrate binding. The present work therefore highlights the importance of higher oxidation states of manganese over nuclearity for the development of better *in vitro* catalysts. Besides, an extensive effort has been made to visualize and quantify all supramolecular interaction present in **1** and **2**.

## Introduction

Scientists have been engaged to develop cost-efficient chemicals at a large scale to solve different needs of civilized society like fuels, polymers, energy, materials, agrochemicals and many other industrial products. Enhancement in the field of pharmaceutical and medical applications also needs synthesis of new organic molecules with unique molecular architectures.<sup>1-14</sup> Therefore, the design and synthesis of different catalysts are challenging tasks in the view point of developing new industrial technologies and subsequently facilitating the advancement of science in several key directions. Exploration of mechanistic studies at each stage help to uncover the intriguing nature of catalytic transformations, which further helps to develop more efficient and selective catalytic systems. Selective oxidation of organic molecules plays a crucial role in many biological and industrial processes. Nature has developed several metalloenzymes to fulfil such transformations.<sup>15-23</sup> Metalloenzyme catalysed oxidation reactions are highly regio- and stereo-selective, and function under mild and 'green' conditions. Among them, the enzymes which efficiently activate molecular dioxygen at ambient condition have received a great deal of attention in the past decades.<sup>24-26</sup> Subsequently, the metal complexes, which are able to mimic the function of oxidase (oxygenase) enzymes, are very useful choice for the development of new, more efficient, bio-inspired and environment friendly catalysts for *in vitro* oxidation processes. Amongst various oxidase enzymes, phenoxazinone synthase (PHS) is of great interest mainly because of its wide clinical application.<sup>27</sup> Phenoxazinone synthase (PHS) is an enzyme which contains five copper atoms. Actinomycin D is a potent antineoplastic agent that contains phenoxazinone chromophore.<sup>27</sup> The formation of the phenoxazinone chromophore in Actinomycin D is catalysed by PHS. Actinomycin D is an aromatic heterocyclic natural product where 2-aminophenoxazinone chromophore is linked to two cyclic pentapeptides. This is clinically used for treatment of choriocarcinoma, Wilms tumours, rhabdomyosarcoma, and Kaposi's sarcoma.<sup>28</sup> Phenoxazinone synthase was discovered in 1962. The detail mechanistic study of PHS was first done by Tadhg P. Begley and co-workers.<sup>28</sup> They concluded in their work

that there are four possible mechanistic pathways for oxidation of *o*-aminophenol (OAPH) to phenoxazinone via aiminequinone intermediate. In 1991, Simándi *et al.* established that kinetics of OAPH oxidation in presence of a cobalt(II) complex follows Michaelis-Menten type kinetics. In 2008, Hassanein *et al.* showed that OAPH oxidation follows first order kinetics with respect to OAPH involving dioxygen species where the catalyst involved was cobalt(II) phthalocyaninetetrasodiumsulfonate.<sup>29</sup> Till date, several research groups have reported different transition metal complexes which mimics PHS enzyme.<sup>30</sup> However, there are limited studies dealing with structure-property correlation in PHS mimicking complexes specially for Mn(II/III) systems. Coordination compounds derived from Schiff base ligands have provided a large number of synthetic models mainly because of synthetic simplicity.<sup>29</sup> Here, we have used azo appended *o*-vanillin aiming to bring extra stability in the solid-state through different non-covalent interactions such as  $\pi$ - $\pi$  stacking interactions involving appended azo-aromatic part.

Previous studies have studied the ability of azo-aromatic compounds to interact with a variety of systems. For instance, several coordination polymers with different architectures have been designed and synthesized using azobenzenetetracarboxylic acid as ligand. Remarkably, the azo-ligand play an important role in adjusting the structural diversity.<sup>31a</sup> Moreover, it has been recently reported that a novel azo ligand [2,2'-(1,3-phenylenebis(diazene-2,1-diyl))bis(4-chlorophenol)] and its mononuclear Cr(III), Mn(II), Fe(III), Co(II), Ni(II), Cu(II), Zn(II) and Cd(II) complexes present interesting antimicrobial activity.<sup>31b</sup> Similarly, the docking of new organic/inorganic hybrid materials composed of chiral salen-type Schiff base Mn(II), Co(II), Ni(II), Cu(II), and Zn(II) complexes having azobenzene groups and laccase has been recently demonstrated.<sup>31c</sup> In addition, it has been shown that chromium complexes with two positional isomers of 2-[(N-arylamino)phenylazo]pyridine are able to stabilize the metal ion in two different oxidation states. Finally, combined theoretical and experimental studies on azoligands are also available in the literature.<sup>31d</sup> For example Jana *et al.*<sup>31e</sup> have reported the synthesis and X-ray characterization of four ruthenium-PPh<sub>3</sub> complexes with a donor azo-ligand, 1-methyl-2-{{*o*-thiomethyl}phenylazo}imidazole in combination with DFT and TDDFT calculations that were used to characterize the systems.

In this work, we have reported two complexes involving azo Schiff base ligands. The Mn(III) mononuclear complex (**1**) exhibits strong phenoxazinone synthase like activity, whereas Zn(II)-Mn(II) tetranuclear complex (**2**) is found to be feebly active or rather almost inactive. So,

here we have focused on factors governing the reactivity of the complexes. A detail study has been made for structure-property correlation to justify the reactivity trend of the complexes. Besides, supramolecular interactions of the complexes have been computed using TURBOMOLE software. The energetic features of the noncovalent interactions (H-bonding and  $\pi$ - $\pi$  stacking) that govern the supramolecular assemblies observed in the solid state have been studied by means of DFT calculations and MEP analysis.

## Experimental section

### Materials and synthesis

All reagent or analytical grade chemicals and solvents were purchased from commercial sources and used without further purification.

#### Synthesis of (E)-2-hydroxy-3-methoxy-5-(p-tolyldiazenyl)benzaldehyde

The azo aldehyde [(E)-2-hydroxy-3-methoxy-5-(p-tolyldiazenyl)benzaldehyde] has been synthesized using standard procedure.<sup>32</sup> Briefly, 4 mL conc. HCl was added to 15 mL water and kept in an ice bath keeping the temperature 0 °C. To it, *p*-toluidine (4.0 mmol, 0.430 g) was added. To this mixture an aqueous solution of sodium nitrite (6.0 mmol, 0.414 g) was added drop wise over a time period of 30 mins. The mixture was stirred for 1 h at 0 °C and then the resultant solution was added to the alkaline *o*-vanillin (4.8 mmol, 0.730 g) which was kept in another ice bath. The mixture was further stirred for 1 h at 0 °C. The solution was neutralised using dilute HCl and pH was maintained around 7.0. The mixture was extracted with dichloromethane and evaporated to result red coloured aldehyde.

#### Synthesis of Schiff base ligand [ $H_2L^1 = (E)$ -6,6'-((1E,1'E)-(ethane-1,2-diylbis(azanylylidene))bis(methanylylidene))bis(2-methoxy-4-((E)-p-tolyldiazenyl)phenol)]

A mixture of (E)-2-hydroxy-3-methoxy-5-(p-tolyldiazenyl)benzaldehyde (2.0 mmol) and 1,2-diaminoethane (1.0 mmol, 60.1 mg) was heated to reflux for 4 h in methanol-dichloromethane solvent mixture (1:1, v/v). The resulting deep red coloured Schiff base ligand ( $H_2L^1$ ) was used for further complexation reaction.

IR ( $cm^{-1}$ , KBr):  $\nu(C=N)$  1610 m;  $\nu(N=N)$  1400 s.

$^1H$  NMR ( $CDCl_3$ , 300 MHz)  $\delta$  ppm: 2.41 (Ar- $CH_3$ ) (s, 3H), 3.96 (- $OCH_3$ ) (s, 3H), 4.02 (- $CH_2$ ) (s, 2H), 7.26-7.29 (Ar-H) (d, 9Hz, 2 H), 7.53 (Ar-H) (s, 2 H), 7.74-7.77 (Ar-H) (d, 9Hz, 2 H), 8.39 (- $CH=N$ ) (s, 1H), 14.19 (-OH) (bs, 1H).

### Synthesis of Schiff base ligand [ $H_2L^2 = (E)$ -6,6'-((1E,1'E)-((2,2-dimethylpropane-1,3-diyl)bis(azanylylidene))bis(methanylylidene))bis(2-methoxy-4-((E)-p-tolyldiazenyl)phenol)]

A mixture of (E)-2-hydroxy-3-methoxy-5-(p-tolyldiazenyl)benzaldehyde (2.0 mmol) and 2,2-dimethyl-1,3-diaminopropane (1.0 mmol, 0.102 g) was heated to reflux for 4 h in methanol-dichloromethane solvent mixture (1:1, v/v). The resulting deep red coloured Schiff base ligand ( $H_2L^2$ ) was used for further complexation reaction.

IR ( $cm^{-1}$ , KBr):  $\nu(C=N)$  1616 m;  $\nu(N=N)$  1390 s.

$^1H$  NMR ( $CDCl_3$ , 300 MHz)  $\delta$  ppm: 1.15 (- $CH_3$ ) (s, 3H), 2.42 (Ar- $CH_3$ ) (s, 3H), 4.00 (- $OCH_3$ ) (s, 3H), 3.40 (- $CH_2$ ) (s, 2H), 7.27 (Ar-H) (s, 2 H), 7.57 (Ar-H) (s, 2 H), 7.75-7.8 (Ar-H) (m, 2 H), 8.36 (- $CH=N$ ) (s, 1H).

### Preparation of $[Mn^{III}(L^1)Cl(H_2O)].H_2O(1)$

A 10 mL methanolic solution of manganese(II) chloride tetrahydrate (1.0 mmol, 0.198 g) was added drop wise to  $CH_2Cl_2$ /methanol (1:3, v/v) solution of  $H_2L^1$  (1.0 mmol) followed by addition of triethylamine (2.0 mmol, ~0.28 mL), and the resultant reaction mixture was heated to reflux for about 1 h. The solution was then cooled and filtered. Deep brown coloured block shaped crystals resulted from the slow evaporation of methanolic solution of the complex at room temperature. Yield: 0.613 g (89%). Anal. Calc. for  $C_{32}H_{34}ClMnN_6O_6$ : C 55.78%; H 4.97%; N 12.20%. Found: C 55.65%; H 4.77%; N 12.08%. IR ( $cm^{-1}$ , KBr):  $\nu(C=N)$  1625 m;  $\nu(N=N)$  1425 s;  $\nu(C-H)$  730 s. UV-Vis,  $\lambda_{max}$  (nm), ( $\epsilon$  ( $dm^3 mol^{-1} cm^{-1}$ )) in MeOH: 227 (88920), 294 (35877), 391 (16047).

### Preparation of $\{Zn^{II}_2(L^2)_2Cl_2\}Mn^{II}_2(\mu_{1,1}-N_3)_2(H_2O)_2\}.2H_2O(2)$

A 5 mL methanolic solution of zinc(II) chloride (1.0 mmol, 0.136 g) was added drop wise to  $CH_2Cl_2$ /methanol (1:3, v/v) solution of  $H_2L^2$  (1.0 mmol) followed by addition of triethylamine (2.0 mmol, ~0.28 mL), and the resulting solution was stirred at room temperature for *ca.* 2 h. To the resulting mixture, 5 mL methanolic solution of manganese(II) chloride tetrahydrate (1.0 mmol, 0.198 g) was added drop wise followed by gradual addition of aqueous methanolic solution (~1.5 mL) of sodium azide (1.00 mmol, 0.065 g). The reaction mixture was then heated to reflux for about 4 h. The solution was then cooled and filtered. Deep bronze coloured plate shaped crystals resulted from the slow evaporation of solution at room temperature. Yield: 1.576 g (92%). Anal. Calc. for  $C_{70}H_{84}Cl_2Mn_2N_{18}O_{14}Zn_2$ : C 49.08%; H 4.94%; N 14.72%. Found: C

49.01%; H 4.85%; N 14.65%. IR ( $\text{cm}^{-1}$ , KBr):  $\nu(\text{N}_3)$  2070 s;  $\nu(\text{C}=\text{N})$  1622 s;  $\nu(\text{N}=\text{N})$  1463s;  $\nu(\text{C}-\text{H})$  768 s. UV-Vis,  $\lambda_{\text{max}}$  (nm), ( $\epsilon$  ( $\text{dm}^3\text{mol}^{-1}\text{cm}^{-1}$ )) in MeOH: 285 (40112), 381 (69492).

### Physical measurements

Elemental analysis for C, H and N was carried out using a Perkin–Elmer 240C elemental analyser. Infrared spectra ( $400\text{--}4000\text{ cm}^{-1}$ ) were recorded from KBr pellets on a Nicolet Magna IR 750 series-II FTIR spectrophotometer. Absorption spectra were measured using a Cary 60 spectrophotometer (Agilent) with a 1-cm-path-length quartz cell. Electron spray ionization mass (ESI-MS positive) spectra were recorded on a MICROMASS Q-TOF mass spectrometer. Measurements of  $^1\text{H}$ NMR spectra were conducted using a Bruker 300 spectrometer in  $\text{CDCl}_3$ . The X-band EPR spectra were recorded using a JEOL JES-FA 200 instrument at liquid nitrogen temperature (77 K). Cyclic voltammetric experiment was performed using a PC-controlled PAR model 273A electrochemical system under nitrogen atmosphere using a Ag/AgCl reference electrode, with a Pt disk working electrode and a Pt wire auxiliary electrode in acetonitrile containing supporting electrolyte, 0.1 M  $\text{Bu}_4\text{NClO}_4$ .

### X-ray crystallography

Single crystal X-ray data of complexes **1** and **2** were collected on a Bruker SMART APEX-II CCD diffractometer using graphite monochromated Mo  $K\alpha$  radiation ( $\lambda = 0.71073\text{ \AA}$ ) at room temperature. Data processing, structure solution, and refinement were performed using Bruker Apex-II suite program. All available reflections in  $2\theta_{\text{max}}$  range were harvested and corrected for Lorentz and polarization effects with Bruker SAINT plus.<sup>33</sup> Reflections were then corrected for absorption, inter-frame scaling, and other systematic errors with SADABS.<sup>34</sup> The structures were solved by the direct methods and refined by means of full matrix least-square technique based on  $F^2$  with SHELX-2017/1 software package.<sup>35</sup> All the non-hydrogen atoms were refined with anisotropic thermal parameters. All the C–H hydrogen atoms were inserted at geometrically idealized positions with  $U_{\text{iso}} = 1/2U_{\text{eq}}$  to those they are attached. Crystal data and details of data collection and refinement for **1** and **2** are summarized in Table 1. The four *p*-tolylmethanimine groups present in the asymmetric unit in **2** have been split over two complementary different positions in order to model the E/Z conformations that are possible conformations for the imino group. To do that, DFIX, DANG and FLAT restraints have been used to keep the molecule integrity during the refinement. The occupancies of the disordered parts were allowed to freely

refine until a constant number was obtained and then the values were changed to fixed ones in order to simplify the final refinement.

**Table1 Crystal parameters and selected refinement details for compounds 1 and 2**

Compound	compound_1	compound_2
CCDC	CCDC 1478366	CCDC 1562304
Formula	C <sub>32</sub> H <sub>34</sub> ClMnN <sub>6</sub> O <sub>6</sub>	C <sub>70</sub> H <sub>84</sub> Cl <sub>2</sub> Mn <sub>2</sub> N <sub>18</sub> O <sub>14</sub> Zn <sub>2</sub>
<i>D</i> <sub>calc.</sub> / g cm <sup>-3</sup>	1.447	1.439
<i>m</i> /mm <sup>-1</sup>	0.556	1.051
Formula Weight	689.04	1713.07
Colour	brown	bronze
Shape	block	plate
Size/mm <sup>3</sup>	0.38×0.20×0.05	0.30×0.16×0.06
<i>T</i> /K	150(2)	150(2)
Crystal System	Monoclinic	Monoclinic
Flack Parameter	.	.
Hoofit Parameter	.	.
Space Group	<i>P</i> 2 <sub>1</sub> / <i>c</i>	<i>P</i> 2/ <i>c</i>
<i>a</i> /Å	20.2205(15)	8.3750(2)
<i>b</i> /Å	12.0071(8)	14.7703(4)
<i>c</i> /Å	13.1850(10)	31.9870(9)
<i>a</i> <sup>o</sup>	90	90
<i>b</i> <sup>o</sup>	98.761(3)	92.0290(10)
<i>g</i> <sup>o</sup>	90	90
<i>V</i> /Å <sup>3</sup>	3163.8(4)	3954.35(18)
<i>Z</i>	4	2
<i>Z</i> '	1	0.5
Wavelength/Å	0.71073	0.71073
Radiation type	MoK <sub>α</sub>	MoK <sub>α</sub>
<i>Q</i> <sub>min</sub> <sup>o</sup>	1.979	1.274
<i>Q</i> <sub>max</sub> <sup>o</sup>	26.467	25.708
Measured Refl.	17653	45338
Independent Refl.	6454	7512
Reflections Used	3895	5586
<i>R</i> <sub>int</sub>	0.0462	0.0347
Parameters	430	610
Restraints	2	287
Largest Peak	1.210	1.315
Deepest Hole	-0.451	-0.872
GooF	1.041	1.055
<i>wR</i> <sub>2</sub> (all data)	0.2284	0.1995
<i>wR</i> <sub>2</sub>	0.1815	0.1815
<i>R</i> <sub>1</sub> (all data)	0.1248	0.0830
<i>R</i> <sub>1</sub>	0.0676	0.0613

### Catalytic oxidation of *o*-aminophenol

Phenoxazinone synthase like activity of the complexes were examined by the reaction of  $1.0 \times 10^{-5}$  M dioxygen-saturated methanolic solutions of the complexes with  $10^{-2}$  M solution of *o*-aminophenol (OAPH) at 25 °C. Upon formation of the phenoxazinone chromophore, the successive increase in absorbance band at *ca.* 433 nm was monitored spectrophotometrically. To evaluate the rate dependency of the reaction on OAPH concentration and to evaluate various kinetic parameters like  $V_{\max}$ ,  $K_M$ ,  $K_{\text{cat}}$ ,  $1.0 \times 10^{-5}$  (M) solution of the complexes were mixed with various concentration of substrate maintaining minimum 10 folds excess to that of catalyst to retain the pseudo-first-order condition. Rate of a reaction was evaluated from the initial rate method, and the average initial rate over three independent measurements was recorded.

### Theoretical methods

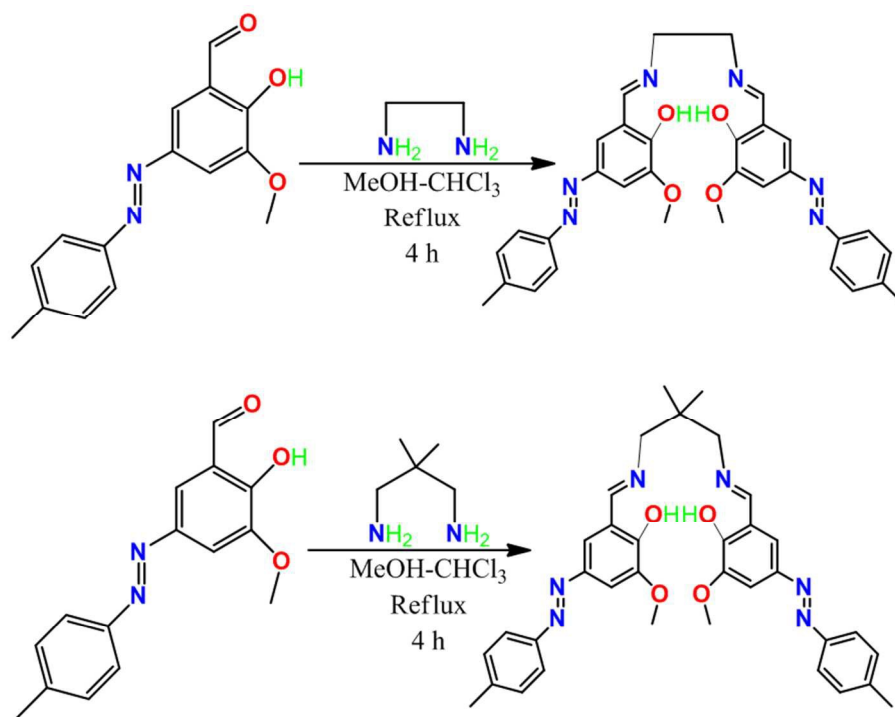
The calculations of the noncovalent interactions were carried out using the TURBOMOLE version 7.0<sup>36</sup> using the M06-2X/def2-TZVP level of theory. To evaluate the interactions in the solid state, we have used the crystallographic coordinates. This procedure and level of theory have been successfully used to evaluate similar interactions.<sup>37</sup> The interaction energies were computed by calculating the difference between the energies of isolated monomers and their assembly. The interaction energies were corrected for the Basis Set Superposition Error (BSSE) using the counterpoise method.<sup>38</sup>

### Results and Discussion

#### Syntheses and spectral characterization of ligands ( $H_2L^1$ and $H_2L^2$ ) and complexes 1 and 2

Initially, azoaldehyde has been prepared by diazo-coupling reaction between *p*-toluidine and *o*-vanillin.<sup>32</sup> Then Schiff bases have been synthesized through condensation of diamines with that azoaldehyde in a 1:2 molar ratio in reagent grade methanol-dichloromethane solvent mixture (Scheme 1). Azoaldehyde and Schiff base ligands have been initially characterized by CHN analysis and ESI Mass spectroscopy. In <sup>1</sup>HNMR spectrum of  $H_2L^1$  ( $CDCl_3$ ), imine proton appeared at 8.39 ppm. Aromatic, aliphatic and methoxy protons appeared at 7.26–7.77 ppm, 4.02 ppm, and 3.96 ppm, respectively. The aromatic–OH appeared at 14.19 as a broad singlet. Hydrogen atoms of methyl group of toluidine ring appeared at 2.41 ppm (Fig. S1). In <sup>1</sup>HNMR spectrum of  $H_2L^2$  ( $CDCl_3$ ), imine proton appeared at 8.36 ppm. Aromatic, aliphatic –CH<sub>2</sub>, –CH<sub>3</sub>

and methoxy protons appeared at 7.27–7.78 ppm, 3.40 ppm, 1.15 ppm, and 4.00 ppm, respectively (Fig. S2). Methyl protons of toluidine appeared at 2.42 ppm. The bands appearing at 1610  $\text{cm}^{-1}$  and 1616  $\text{cm}^{-1}$ , respectively, are the characteristic stretching frequency of  $-\text{CH}=\text{N}$  bonds of both of the schiff base ligands. Whereas bands appearing at 1400  $\text{cm}^{-1}$  and 1390  $\text{cm}^{-1}$ , respectively, are the characteristic stretching frequency of azo bonds ( $\text{N}=\text{N}$ ) of both of the schiff base ligands (Figs. S3 and S4). For complexes **1** and **2**, the bands appeared in the IR spectra around 1600 and 1620  $\text{cm}^{-1}$ , respectively, are assigned to  $-\text{CH}=\text{N}$  stretching frequency. Whereas, the characteristic azo  $\text{N}=\text{N}$  stretching frequency of complexes **1** and **2** are obtained around 1445 and 1460  $\text{cm}^{-1}$ , respectively. The characteristic  $\mu$ -1,1 azido stretching of complex **2** has been obtained at around 2070  $\text{cm}^{-1}$  (Figs. S5 and S6). All the characteristic stretching frequencies of FTIR data are very much comparable with that of literature values.<sup>39</sup> UV-Vis spectra of complexes **1** and **2** have been recorded in methanol solvent at room temperature. Complex **1** shows absorption bands around 391, 294 and 227 nm attributed to  $n \rightarrow \pi^*$  transitions and  $\pi \rightarrow \pi^*$  transitions, respectively. Whereas, complex **2** shows absorption bands around 380 nm and 285 nm attributed to  $n \rightarrow \pi^*$  transitions and  $\pi \rightarrow \pi^*$  transitions, respectively.



Scheme 1. The route to the syntheses of ligand  $\text{H}_2\text{L}^1$  and  $\text{H}_2\text{L}^2$ .

### Description of the crystal structure of **1**

The X-ray data reveal that complex **1** crystallized in the monoclinic  $P2_1/c$  space group. Crystal structure of complex **1** is depicted in Fig. 1. Selected bond distances and bond angles are listed in Table 2. The Mn(III) complex is mononuclear and the metal centre is hexa-coordinated, where secondary valence has been satisfied by two imine-N atoms and two phenoxido-O atoms of the tetradentate Schiff base ligand, one chloride ion and one water molecule, respectively. There is another molecule of water present in the crystal system which was contained by non-dried solvent (methanol), used for crystallization purpose. The tri-positive charges of Mn(III) ion have been satisfied by the dianionic tetra dentate ligand and one chloride ion. The geometry around the manganese centre is best described as a slightly distorted octahedron.

**Table 2.** Selected bond lengths (Å) and bond angles (°) for complex **1** at 150 K.

Mn-N1	1.980(4)	N1-Mn-N2	82.75(15)
Mn-N2	1.975(4)	N1-Mn-O1	91.49(14)
Mn-O1	1.889(3)	N2-Mn-O2	91.49(15)
Mn-O2	1.891(3)	O3-Mn-Cl	170.06(10)
Mn-Cl	2.5407(15)		
N3-N4	1.260(6)		
N5-N6	1.229(7)		
Mn-O3	2.277(4)		
Cl-O100	3.317(6)		

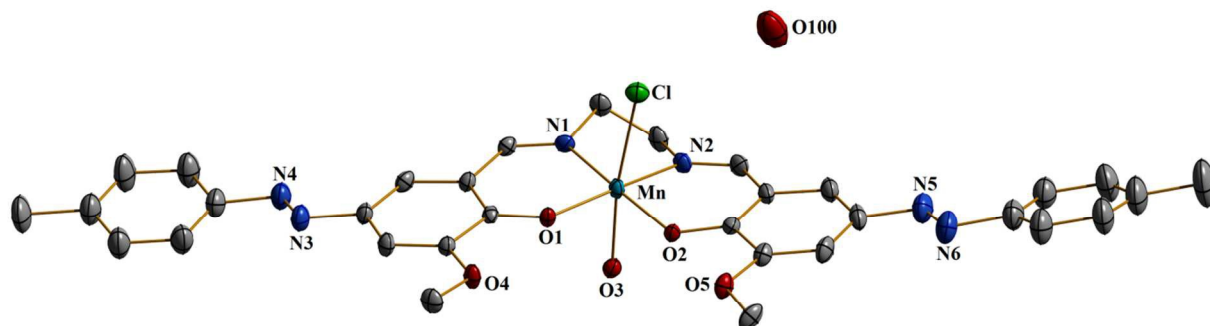


Fig. 1. Ortep view of complex 1. Atoms are shown as 30% thermal ellipsoids. H atoms are omitted for clarity.

In the said octahedron environment, the equatorial sites are occupied by imino-N atoms and phenoxido-O atoms, respectively, and the axial sites are occupied by chloride ion and water molecule. It has been found that manganese centre deviates from the mean basal plane by 0.095 Å. The Mn–N<sub>imino</sub> and Mn–O<sub>phenoxido</sub> bond distances of the Schiff base are found to be 1.980(4) Å (Mn–N1), 1.975(4) Å (Mn–N2), 1.889(3) Å (Mn–O1), and 1.891(3) Å (Mn–O2), which are comparable with that of previously reported literature values.<sup>40</sup> The Mn<sup>III</sup>–Cl and Mn<sup>III</sup>–OH<sub>2</sub> axial bond distances are 2.5407(15) Å and 2.277(4) Å, respectively, that are typical for the elongated Jahn Teller distortion around the Mn(III) ion (d<sup>4</sup> system), while azo N=N bond distance is found to be ~ 1.2 Å. The bite angles of the complex are 82.75(15)° (N1–Mn–N2), 91.49(14)° (O1–Mn–N1) and 91.49(15)° (O2–Mn–N2) respectively. The value of transoid angle is 170.06(10)° (O3–Mn–Cl). The Cl atom is tilted toward the O atom of the second sphere water molecule [Cl···O distance 3.317(6) Å].

It is curious that a water ligand is placed at the first coordination sphere, instead of the most abundant MeOH molecule that is used as solvent. In fact, this was the case for a related pyridoxal-derived Schiff base Mn(III) complexes reported by Naskar et al.<sup>40b</sup> displaying trans-oriented Cl/MeOH ligands in a similar environment. Probably equilibrium of both complexes exists in the mother solution and, for some reason, only the water coordinated complex crystallizes displacing the equilibrium.

## Description of the crystal structures of 2

Single crystals of complex **2** were obtained from slow evaporation of its solvent mixture of dichloromethane-methanol. It crystallized with the  $P2_1/c$  space group in the monoclinic unit cell. Crystal structure of complex **2** is depicted in Fig. 2. Selected bond distances and bond angles are listed in Table 3. Complex **2** is a centrosymmetric tetranuclear molecule, where the asymmetric unit contains  $[Zn(L^2)(Cl)Mn(H_2O)(\mu_{1,1}-N_3)]$  moiety which through symmetry operation generates the whole molecule. Asymmetric units are connected by two symmetry related  $\mu_{1,1}$  azido bridges resulting in a formation of this tetranuclear molecule. In the asymmetric unit, the inner core of the azo bicompartamental Schiff base ligand is occupied by zinc(II) ion and outer core is occupied by Mn(II) ion. The Zn(II) ion placed in the inner core of the ligand is penta-coordinated with two phenoxido-O atoms, two imine-N atoms and one chloride ion. The geometry index (structural or Addison parameter) ( $\tau$ )<sup>41</sup> for Zn(II) centre is found to be 0.046 which is very close to zero and the environment around the Zn(II) centre suggests to be almost square pyramidal. Here,  $\tau = \frac{\alpha - \beta}{60}$ ,  $\alpha$  and  $\beta$  being the two greatest valence angles of the coordination centre. The equatorial sites of the penta-coordinated Zn(II) ion are occupied by two imino-N atoms and two phenoxido-O atoms. The Zn–N<sub>imino</sub> and Zn–O<sub>phenoxido</sub> bond distances are 2.093(5) Å (Zn1–N3), 2.048(6) Å (Zn1–N25), 2.018(4) Å (Zn1–O7) and 2.069(3) Å (Zn1–O29). The apically coordinated Zn–Cl bond distance is 2.257(2) Å. The Zn(II) ion deviates from mean N<sub>2</sub>O<sub>2</sub> plane by 0.503 Å. The Mn(II) ion placed in the outer core is connected with the Zn(II) ion through two phenoxido bridges. The secondary valence of Mn(II) centre is satisfied by two bridging phenoxido-O atoms, two methoxy-O atoms, two bridging ( $\mu_{1,1}$ ) azido ions and one water molecule. The Mn(II) centre is hepta-coordinated and adopts a distorted pentagonal bipyramidal geometry. In the coordination sphere it is equatorially coordinated with two phenoxido-O atoms (O7, O29), two methoxy-O atoms (O9, O31) and a  $\mu_{1,1}$  bridged azido nitrogen atom (N46). Whereas, oxygen atom of a water molecule (O1W) and a symmetry related  $\mu_{1,1}$  bridged azido nitrogen atom (N46A) are axially coordinated with the metal centre. It has been observed that the Mn(II) is slightly above (0.018 Å) the pentagonal plane. The value of transoid angle is 169.45(15)° (O1W–Mn1–N46A). The Mn<sup>II</sup>–O<sub>phenoxido</sub>, Mn<sup>II</sup>–O<sub>methoxy</sub>, Mn<sup>II</sup>–N<sub>azido</sub> and Mn<sup>II</sup>–O<sub>water</sub> bond distances are found to be 2.166(3)Å (Mn1–O7), 2.160(3)Å (Mn1–O29), 2.452(4)Å (Mn1–O9), 2.499(3)Å (Mn1–O31), 2.200(4)Å (Mn1–N46) and 2.157(4)Å (Mn1–O1W), respectively. The Zn(II)⋯Mn(II) and Mn(II)⋯Mn(II) separations are 3.381 Å and 3.495

Å respectively. All the bond distances around Zn(II) and Mn(II) centres are found to be comparable with that of previously reported literature values.<sup>42</sup> The Mn1-( $\mu_{1,1}$ )N1-Mn1A angle is found to be 104.06(14)°. Two water molecules are present as solvents of crystallization in the given crystal system. The azo N=N bond distances are found to be 1.06(1) Å (N14-N15) and 1.02(1) Å (N36-N37). The pictorial representation of coordination environment around the metal centre is given in Fig. S7. The value of bite angles around Zn(II) and Mn(II) centres are 94.8(2)° (N3-Zn1-N25), 88.27(17)° (N3-Zn1-O7), 88.03(19)° (N25-Zn1-O29), 66.88.(13)° (O7-Mn1-O9), 70.40(13)° (O7-Mn1-O29) and 67.17(12)° (O29-Mn1-O31), respectively.

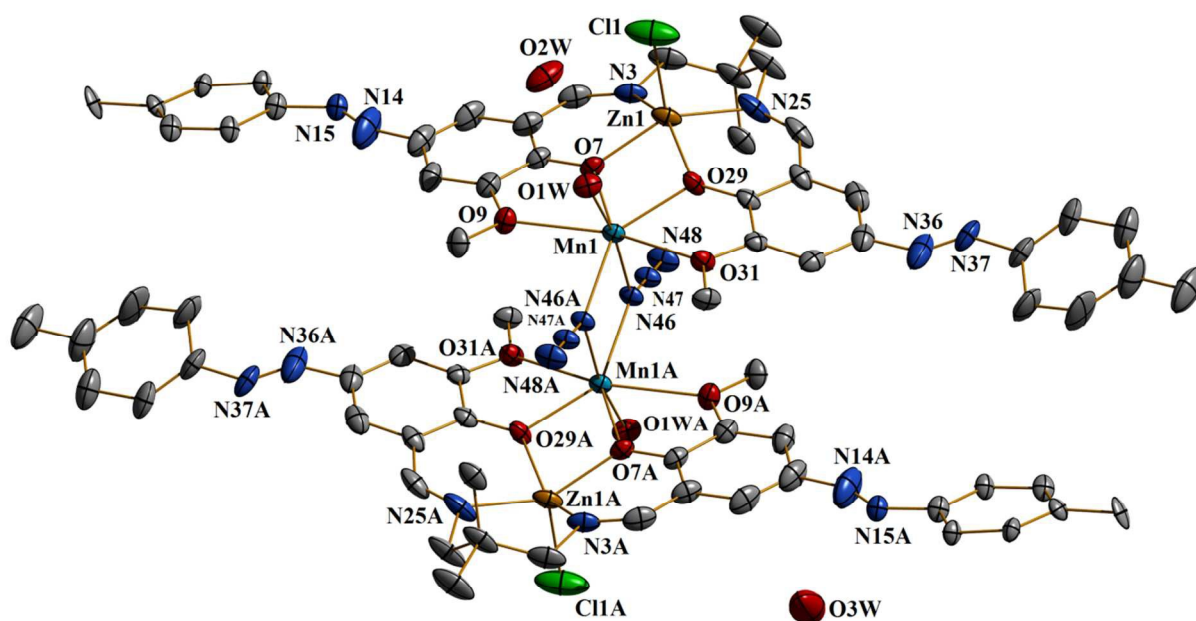


Fig. 2. Ortep view of complex 2. Atoms are shown as 30% thermal ellipsoids. H atoms are omitted for clarity. [Symmetry operation: A = -x, -y, -z].

**Table 3.** Selected bond lengths (Å) and bond angles (°) for complex **2** at 150 K.

Zn1-N3	2.093(5)	Mn1-Mn1	3.495
Zn1-N25	2.048(6)	N25-Zn1-N3	94.8(2)
Zn1-O7	2.018(4)	O7-Zn1-N3	88.27(17)
Zn1-O29	2.069(3)	O29-Zn1-N25	88.03(19)
Zn1-Cl1	2.257(2)	O7-Mn1-O9	66.88(13)
N14-N15	1.06(1)	O7-Mn1-O29	70.40(13)
N36-N37	1.02(1)	O29-Mn1-O31	67.17(12)
Mn1-O7	2.166(3)	O1W-Mn1-N46	169.45(15)
Mn1-O9	2.452(4)	Mn1-N46-Mn1A	104.01(2)
Mn1-O29	2.160(3)	N46-N47-N48	179.8(7)
Mn1-O1W	2.157(4)		
Mn1-N46	2.200(4)		
Mn1-O31	2.499(3)		

### Computational Study

The theoretical study is devoted to analyse some noncovalent interactions that are present in the crystal packing of Mn(III/II) complexes **1** and **2** focusing our attention to the role of the coordinated water ligand influencing the crystal packing of **1**. As a first approximation we computed the Molecular Electrostatic Potential (MEP) surface of complex **1** in order to analyse its electron donor/acceptor properties. It can be observed that the most positive region corresponds to the H-atoms of coordinated water molecule due to the enhanced acidity of these protons as a consequence of the metal coordination. Moreover, the most negative region corresponds to the phenoxide O atoms. In fact the four O atoms (two from the phenoxide groups and two from methoxy groups) converge to the same point, providing an electron rich region. Moreover, the coordinated chlorido ligand also presents a spherical region of negative potential (Fig. 3).

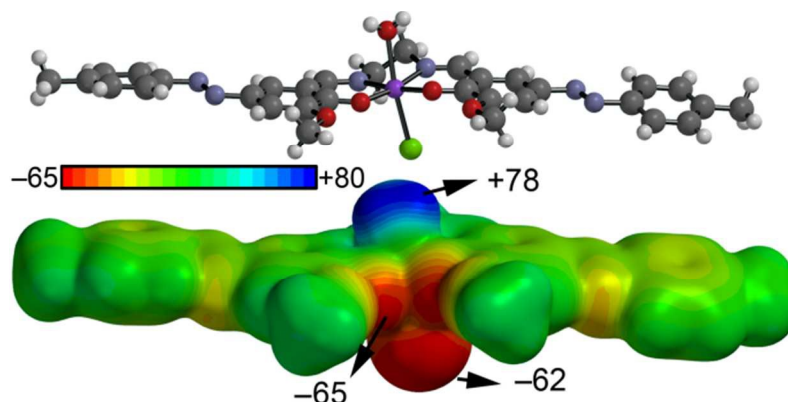


Fig.3. MEP surface of complex **1**. Energies at selected points of the surfaces are given in kcal/mol.

In Fig. 4a we show partial view of the crystal packing (2D-supramolecular chain) of complex **1** where it can be observed the presence of self-assembled dimers. We have analysed these dimers in detail (Fig. 4b) and coordinated water molecule establishes four H-bonding interaction with the oxygen atoms of the Schiff base ligand, in sharp agreement with the MEP analysis shown in Fig. 3. We have evaluated the binding energy of this dimer, which is very large and negative ( $\Delta E_1 = -75.1$  kcal/mol) as a consequence of the formation of eight H-bonding interactions and confirms the relevance of these interactions in the crystal packing of complex **1**. Moreover, this self-assembled dimer also present two different types of  $\pi$ -stacking interactions, one between the uncoordinated rings (4.08 Å) and the other between the coordinated rings (3.61 Å) of the ligand. In order to evaluate the contribution of the H-bonds, we have computed a theoretical model where we have eliminated the coordinated water molecules. As a result, the interaction energy is reduced to  $\Delta E_2 = -37.4$  kcal/mol and the contribution of the H-bonds can be estimated as the difference,  $\Delta E_1 - \Delta E_2 = -27.7$  kcal/mol. In an effort to evaluate the  $\pi$ -stacking interactions between the uncoordinated rings, we have computed an additional model where the rings have been eliminated. Thus, the energy is reduced to  $\Delta E_3 = -22.3$  kcal/mol and consequently a rough estimation of the contribution of each stacking interaction is  $1/2(\Delta E_3 - \Delta E_2) = -7.6$  kcal/mol (Fig. 4c-d).

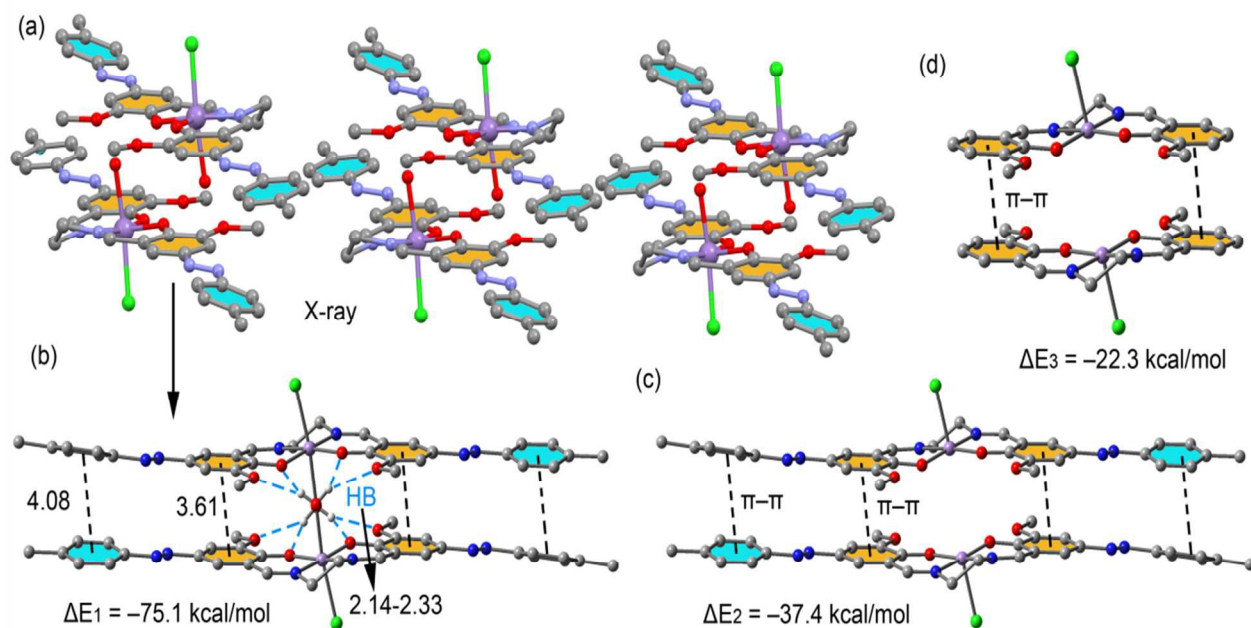


Fig.4.(a) X-ray fragment of **1**.(b-d) theoretical models used to evaluate the noncovalent interactions. H-atoms omitted for clarity apart those involved in the H-bonds. Distances in Å.

In complex **2** we have evaluated the energy of the self-assembled 1D supramolecular chains observed in the solid state which are governed by the formation of symmetrically equivalent O-H $\cdots$ N H-bonds (see Fig.5a). We have computed a dimer extracted from this polymeric chain (Fig.5b) and a close examination reveals the existence of unconventional C-H $\cdots$ Cl H-bonding interactions that also participate in the assembly mechanism (see red dashed lines). We have computed the binding energy of this dimer, which is large and negative ( $\Delta E_4 = -26.2$  kcal/mol) as a consequence of the formation of two strong O-H $\cdots$ N(azide) interactions and four weaker C-H $\cdots$ Cl H-bonding interactions. In an effort to evaluate the contribution of the ancillary C-H $\cdots$ Cl H-bonding interactions, we have used a theoretical model where four methyl groups have been replaced by H atoms (see small arrows in Fig.5c). Consequently, the interaction energy is reduced to  $\Delta E_5 = -22.0$  kcal/mol that corresponds to the contribution of the strong O-H $\cdots$ N hydrogen bonds. Moreover, the additional contribution of the rest of unconventional H-bonds can be estimated as the difference,  $\Delta E_4 - \Delta E_5 = -4.2$  kcal/mol.

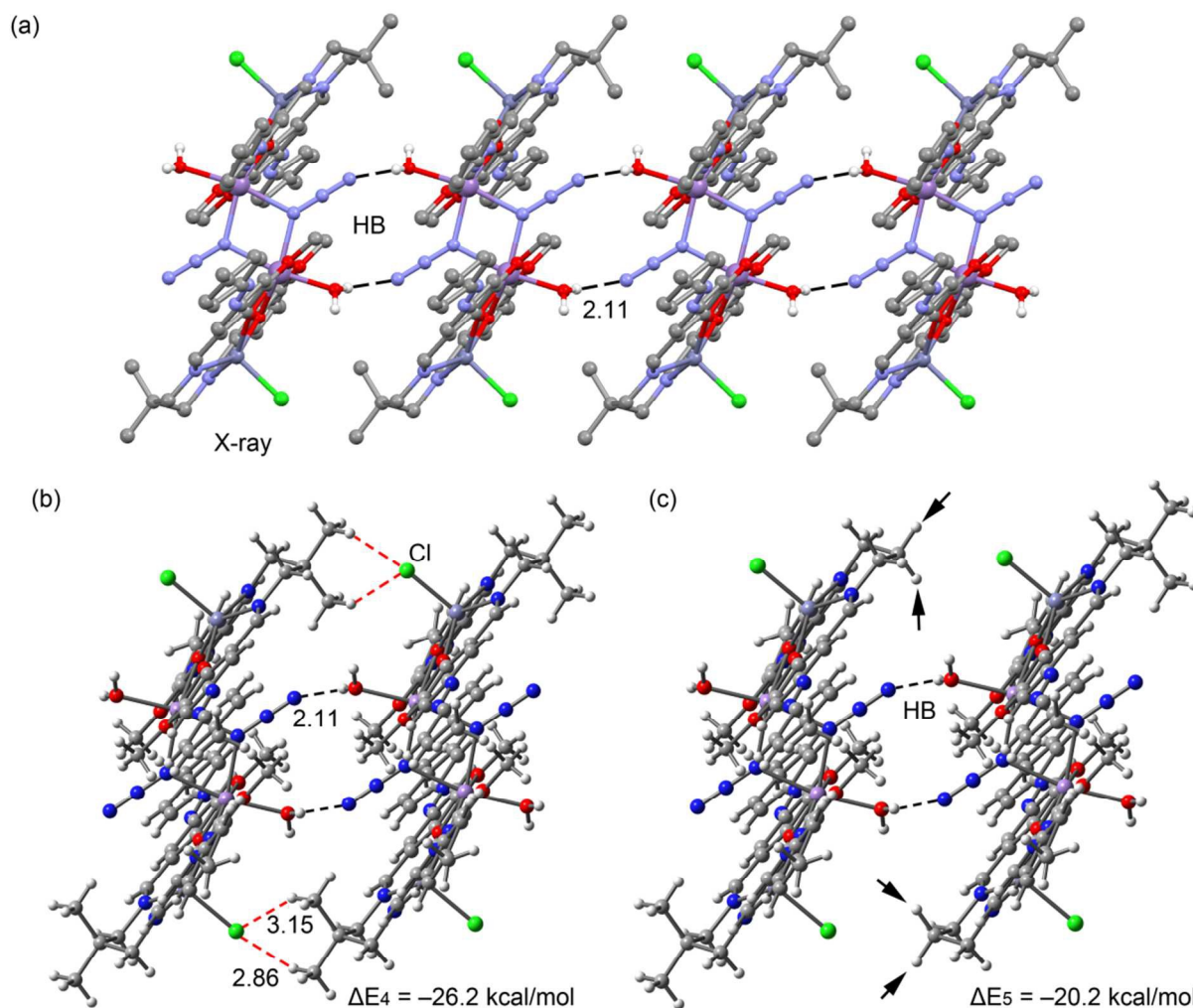


Fig.5. (a) X-ray fragment of **1**, H-atoms omitted for clarity apart those involved in the H-bonds. (b,c) Theoretical models used to evaluate the noncovalent interactions. Distances in Å.

### Electrochemical study

It is well known that the redox flexibility between the different oxidation states of the transition metal at the active site of a metalloenzyme plays an anchoring role in catalysing the oxidation of various biologically important organic molecules. Therefore, it is important to check the electrochemical behaviour of the synthetic compounds as that result could disclose the potential of the synthetic analogues for behaving as redox catalysts. Cyclic voltammogram of complex **1** is depicted in Fig. 6 in which potentials are referenced to the standard Ag/AgCl electrode. An electrochemically irreversible reduction wave was obtained at -0.101 V versus Ag/AgCl

electrode, and this can be assigned to the reduction of manganese(III) to manganese(II).<sup>43</sup> The value of reduction potential (-0.101 V) is found to be very interesting as that suggests that the compound can be capable to oxidase various organic compounds. Furthermore, the reduced manganese(II) species can easily be re-oxidized by the molecular dioxygen. Therefore, the electrochemical study discloses that compound **1** could be an efficient redox catalyst for the aerobic oxidation of various organic compounds. One of such catalytic reaction (phenoxazinone synthase like activity) has been performed in details (*vide infra*).

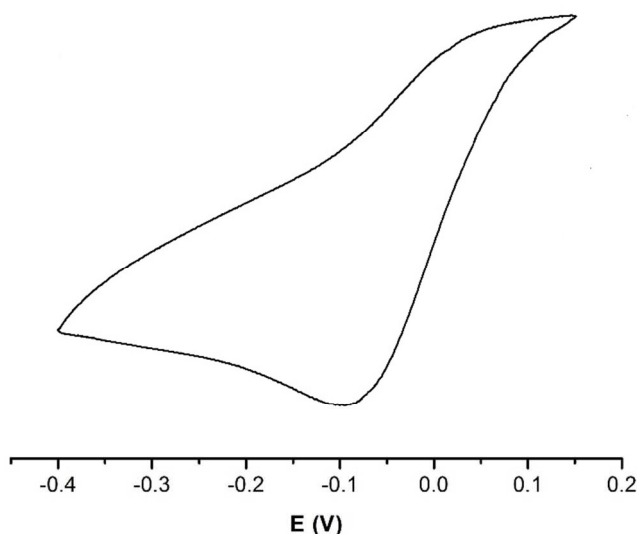


Fig. 6. Cyclic voltammogram of complex **1** in acetonitrile containing TBAP (0.1 M) as a supporting electrolyte at a scan rate of 100 mV/s. Potentials were referenced to the Ag/AgCl couple.

### Phenoxazinone synthase like activity

Catalytic oxidation of *o*-aminophenol (OAPH) was spectrophotometrically studied in dioxygen-saturated methanol solution at 25 °C. Firstly,  $1 \times 10^{-5}$  M methanolic solutions of the complexes were subjected to react with a  $1 \times 10^{-2}$  M solution of OAPH under aerobic condition. Upon successive catalytic oxidation of *o*-aminophenol (OAPH) the characteristic absorbance band of phenoxazinone chromophore at ca. 433 nm gradually increases, which confirms the catalytic activity of the complexes by resulting oxidation of OAPH to 2-aminophenoxazin-3-one in aerobic condition. The time-resolved spectral profiles are shown in Figs. 7 and 8 for **1** and **2**, respectively. A blank experiment has been performed in absence of the each of the complex

(catalyst) under identical condition, which does not result any significant escalation in the band intensity at 433 nm. The outcome of the experiment is that the only complex **1** is catalytically efficient to oxidize OAPH to 2-aminophenoxazin-3-one under aerobic condition. Complex **2** is either feebly active or almost inactive towards OAPH. So, further kinetic study of complex **2** is not required due to its inefficiency to oxidize OAPH to 2-aminophenoxazin-3-one. To have insight view of the reaction kinetics of the complex **1**,  $1 \times 10^{-5}$  M methanolic solutions of the complex were subjected to react with various concentration of substrate maintaining at least 10 folds excess of catalyst used to retain pseudo first order condition. All the kinetic studies have been performed under aerobic condition and at 25 °C temperature maintained using a thermostat. For a particular kinetic study using a specific substrate ratio to that of the complex, time scan at the maximum band (433 nm) of 2-aminophenoxazin-3-one was carried out for a period of 20 min, and initial rate was determined by linear regression from the slope of the absorbance versus time; each experiment was performed thrice and average values were noted. The initial reaction rates versus concentrations of the substrate plot shows rate saturation kinetics as depicted in Fig. 9. These results suggest that, in the catalytic cycle of OAPH oxidation, the complex initially forms adduct with that of the substrate followed by release of oxidized product in an irreversible manner which is the rate determining step (r.d.s.). Since the rate of the reaction depends of substrate concentration only, the following kinetic measurement can be fitted to Michaelis–Menten model. The kinetic parameters *viz.*  $V_{\max}$ ,  $K_M$ , and  $K_{\text{cat}}$  can be determined by linearization of Michaelis–Menten equation which gives double reciprocal Lineweaver–Burk plot. The observed and simulated initial rate versus substrate concentration plot and the Lineweaver–Burk plot for the complexes are shown in Figs. 9 and 10, respectively. Michaelis binding constant ( $K_M$ ) and  $V_{\max}$  were calculated to be  $(6.96 \pm 0.19) \times 10^{-3}$  M and  $9.79 \times 10^{-8}$  M Sec<sup>-1</sup>, respectively. The turnover number ( $K_{\text{cat}}$ ) value is calculated by dividing the  $V_{\max}$  by the concentration of the complex used, and is found to be 35.24 h<sup>-1</sup>. Moreover, linearity has been observed for initial rate of catalysis which confirms pseudo-first order kinetic of the complex **1**.

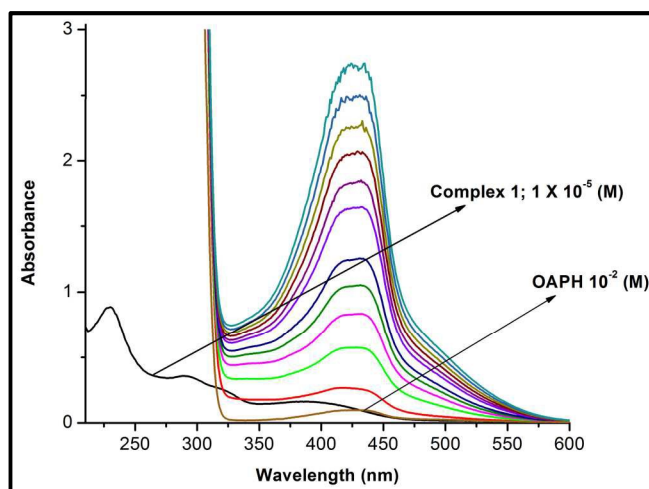


Fig. 7. UV-Vis spectral scans showing the increase in phenoxazinone chromophore band at 433 nm after the addition of *o*-aminophenol ( $10^{-2}$  M) to a solution of complex **1** ( $1 \times 10^{-5}$  M) in methanol at  $25^{\circ}\text{C}$ . The spectra were recorded for the period of 2 h.

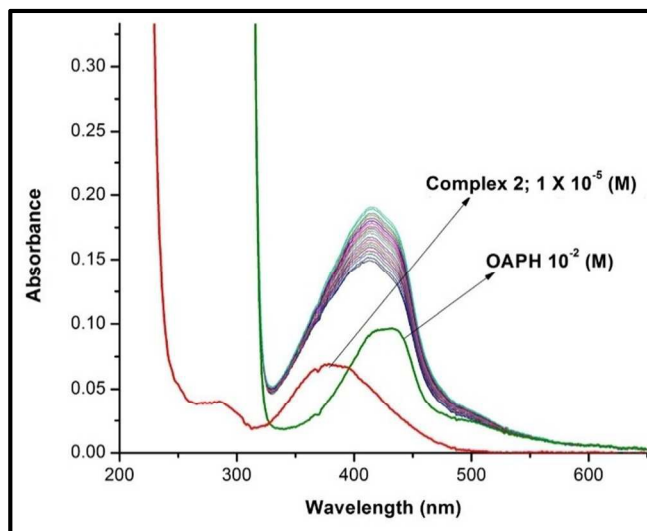


Fig. 8. UV-Vis spectral scans showing the increase in phenoxazinone chromophore band at 433 nm after the addition of *o*-aminophenol ( $10^{-2}$  M) to a solution of complex **2** ( $1 \times 10^{-5}$  M) in methanol at  $25^{\circ}\text{C}$ . The spectra were recorded for the period of 2 h.

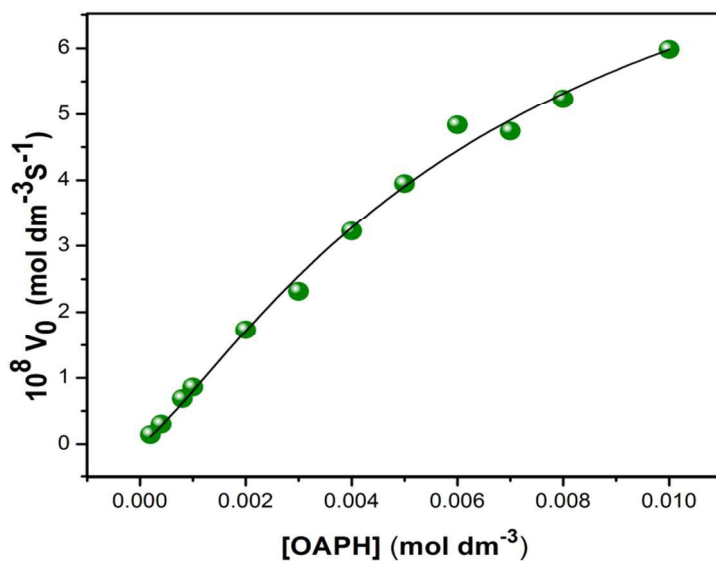


Fig. 9. Initial rate versus substrate concentration plot for the oxidation of *o*-aminophenol catalyzed by complex **1** in dioxygen-saturated methanol. Symbols and solid lines represent the experimental and simulated profiles, respectively.

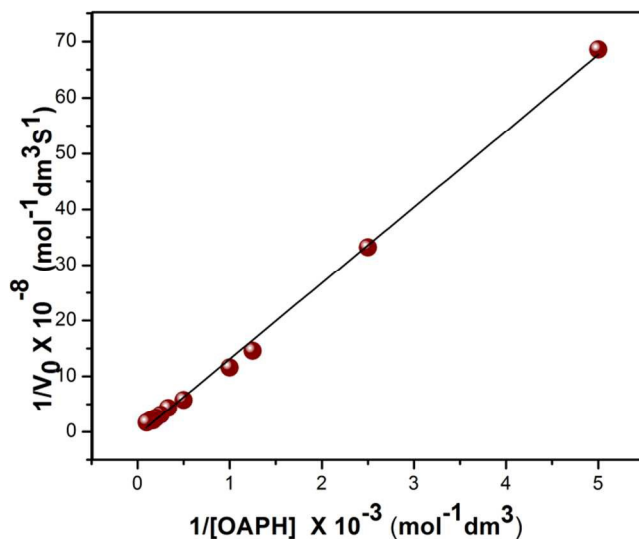


Fig. 10. Lineweaver–Burk plots for the oxidation of *o*-aminophenol catalysed by complex **1** in aerobic condition. Symbols and solid lines represent the experimental and simulated profiles, respectively.

## ESI mass spectral study

Mass spectrometry is a useful technique that could provide significant information regarding the important intermediates of a chemical reaction from which the most possible mechanistic pathway of a catalytic reaction can be framed. As compound **1** is only found active catalyst for the aerobic oxidation of *o*-aminophenol, the ESI (positive) mass spectral studies of compound **1** itself and in the presence of excess of the substrate have been performed in methanol. The mass spectrum of complex **1** (Fig. S8) consists of the base peak at  $m/z = 617.0635$  which can be assigned as the  $[\text{Mn}(\text{L}^1)]^+$  species (calculated  $m/z = 617.17$ ). The second most abundant peak at  $m/z = 338.2629$  is a fragmented molecular ion peak of azoaldehyde together with two water molecules and one methanol molecule (calculated  $m/z = 338.15$ ). When mass spectrum was recorded in presence of excess substrate, the base peak was found at  $m/z = 215.0203$ , which is quite interesting as the isotropic distribution patterns matched well with the protonated intermediate II-B (calculated  $m/z = 215.08$ ) as shown in scheme 2. Again peak at  $m/z = 213.0203$  is a product related peak as that agrees with the protonated species of 2-aminophenoxazin-3-one (calculated  $m/z = 213.06$ ). The basal peak at  $m/z = 617.0635$  in the mass spectrum of the compound itself become a minor component when the mass is ionized in presence of the substrate. Moreover, a minor peak at  $m/z = 726.1697$  related to the complex-substrate aggregate of formula  $[\text{Mn}(\text{L}^1) + \text{OAPH}]^+$  is also deserved to be special mentioned as that suggests binding of the substrate to the metal centre during the catalytic oxidation of the substrate, which is consistent with the rate saturation kinetics (Fig.11).

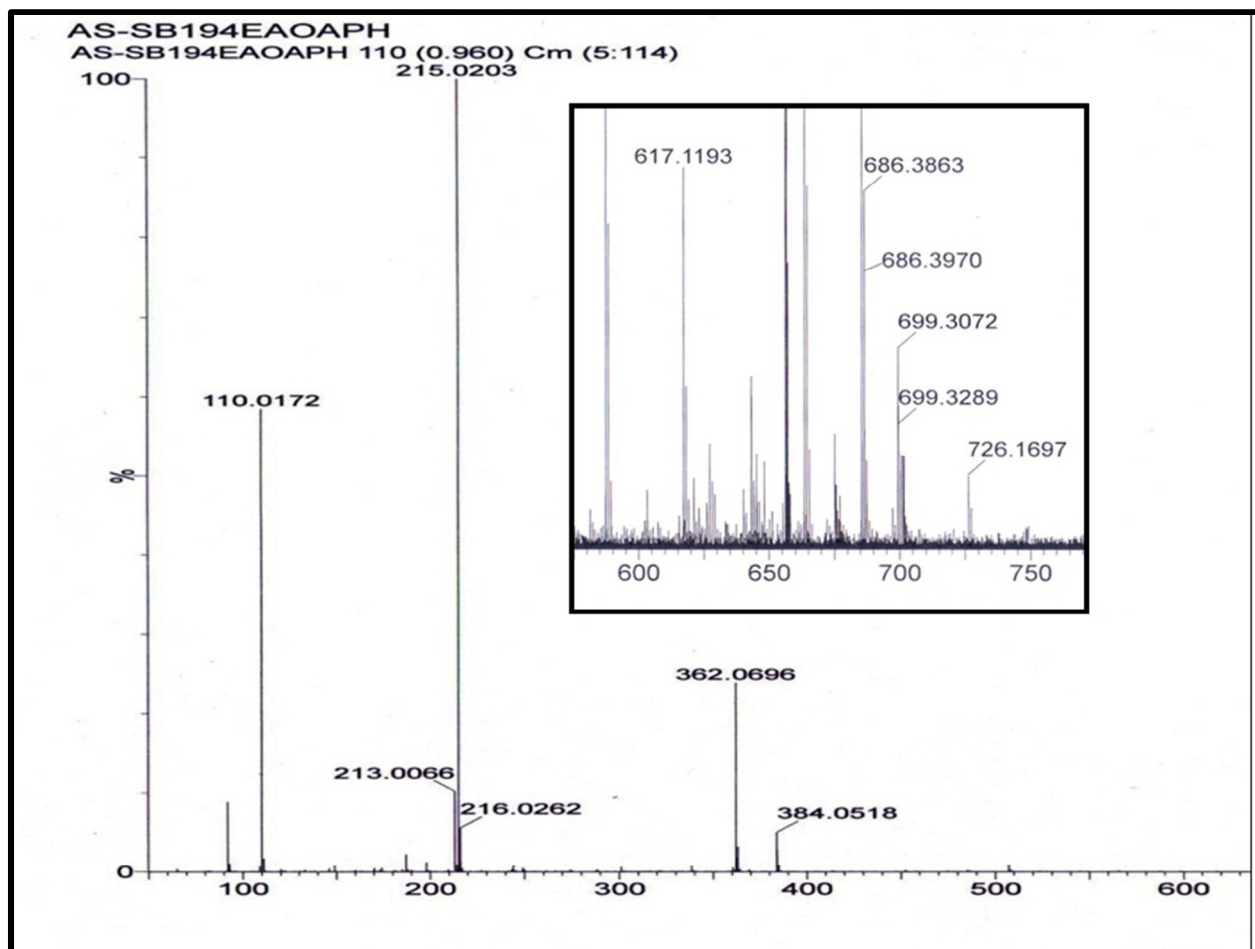


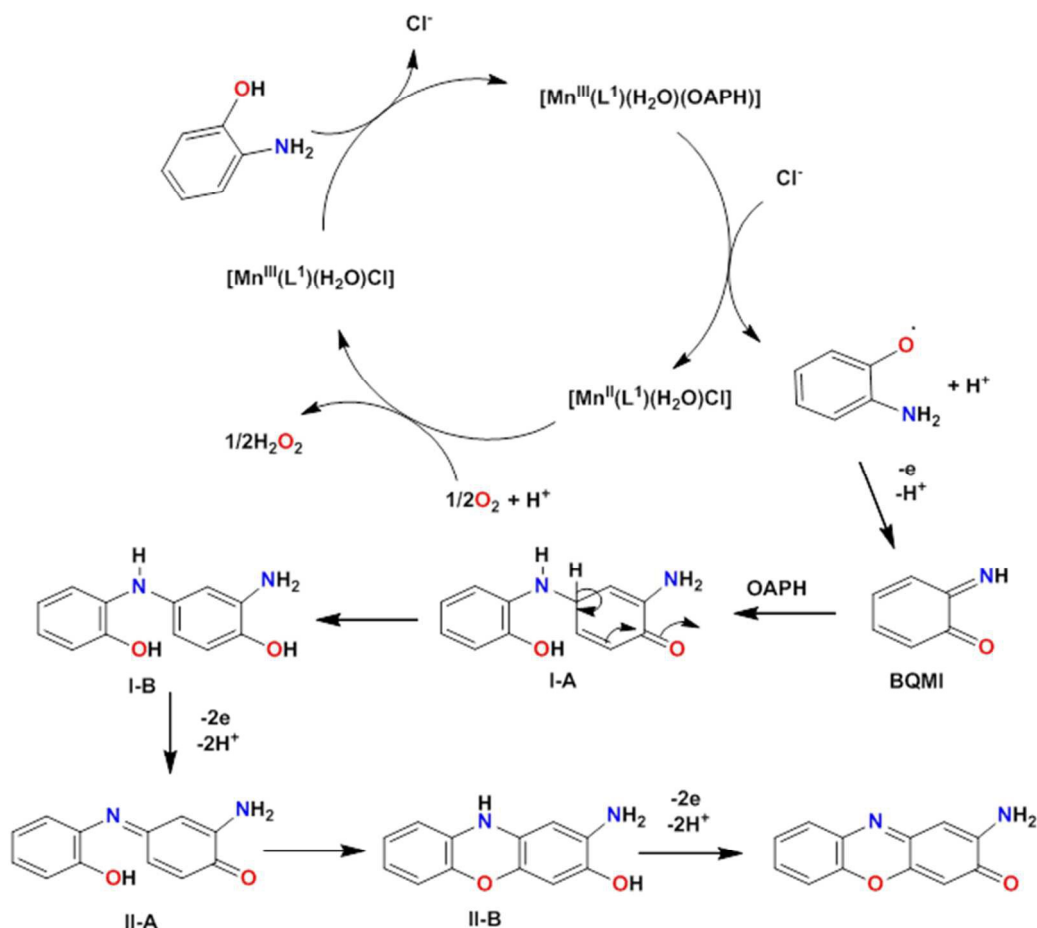
Fig. 11. ESI mass spectrum of complex **1** in presence of excess *o*-aminophenol; Inset showing expanded mass spectrum at selected region.

### Plausible mechanistic pathway and comparative study of catalytic efficiency

Both the rate saturation kinetics and the mass spectral study reveal that the catalytic cycle starts with the formation of a stable complex-substrate aggregate by the replacement of the labile coordinated water or chloride ion at first coordination sphere. It is well known that when the higher oxidation of the transition metal center is involved in the oxidation reaction, it generally oxidises the substrate at the rate determining step and subsequently reduces to the lower oxidation state.<sup>44</sup> In order to check such possibility in our case, we have performed EPR spectroscopic studies. Interestingly, when EPR spectrum was recorded of the complex in presence of excess substrate, we observed six-line EPR spectrum (Fig. 12), which indicates the formation of manganese(II) species in presence of the substrate. The complex itself is found EPR

silent which is characteristic for the manganese(III) complexes. These observations likely suggest that at the first step OAPH forms adduct with the complex **1**, which thereafter through redox transformation generates OAP radical in the rate determining step. Now, the OAP radical might be converted into *o*-benzoquinone monoamine (BQMI) in several ways including self-disproportionation reaction. Finally, 2-aminophenoxazin-3-one is produced through several oxidative dehydrogenation processes involving OAPH, O<sub>2</sub>, and BQMI as shown in Scheme 2. Remarkably, intermediate II-B, shown in Scheme 2, was eventually identified in the mass spectrum of the complex in presence of OAPH, thereby validating the said scheme.

UV-Vis Spectrophotometric study of the catalytic oxidation of OAPH reveals that complex **1** is highly active whereas complex **2** is feebly active or almost inactive. So, here, a structure-property correlation is highly demanded. Catalytic efficiency of a complex depends upon a number of factors viz. oxidation state, nuclearity, binding site, flexibility of ligand system etc. Like **1**, a labile site (coordinated water molecule) is also available at the manganese centre in **2** for substrate binding, and furthermore there are two adjacent manganese(II) centres present in the molecule, still it is found almost unreactive. It can be visualized that when lower oxidation state of the transition metal participates in the catalytic oxidation of the substrate by molecular oxygen, generally, both the substrate binding and dioxygen activation are expected to be required at the rate determining step. In complex **2**, each manganese(II) centre has only one labile site, so either of the two metal centres binds the substrate or molecular dioxygen. Therefore, one can expect that this cooperation may help the catalytic oxidation of substrate by molecular oxygen. In reality, we have found that complex **2** is almost unreactive. Careful inspection of the crystal structure of **2** reveals that two labile water molecules are coordinated to the manganese(II) centres in opposite directions, and consequently two metal-bound reactants dioxygen and OAPH are displayed far away from each other, that rendering the system to have any effect of such cooperation for the substrate oxidation. This result therefore suggests that the proper stereochemical arrangements of the vacant or labile positions in the high nuclearity transition metal complexes are extremely important for the cooperative catalytic activity when lower oxidation state metal ions are involved in aerobic oxidation.



Scheme 2. Probable mechanistic pathway for the formation of the phenoxazinone chromophore catalysed by complex 1.

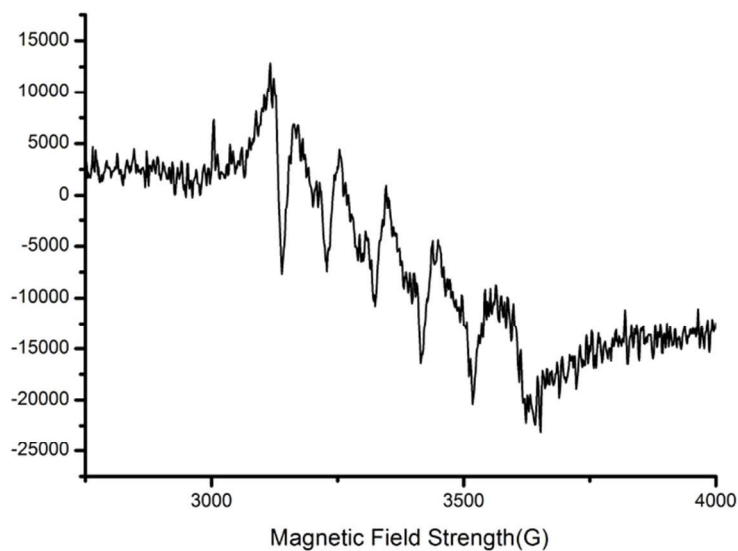


Fig. 12. X-band EPR spectrum of complex 1 after addition of  $\sim 50$  eq. of *o*-aminophenol at 77 K.

## Conclusion

We have synthesized and X-ray crystallographically characterized two new Mn(III/II) complexes **1** and **2**. The azo appended Schiff ligands have been developed for synthesizing metal complexes to introduce  $\pi$ - $\pi$  stacking interactions in the solid state for bringing extra stability in the molecules. The energetic features of the noncovalent interactions that govern the supramolecular assemblies observed in the solid state interactions have been studied by means of DFT calculations and MEP analysis, which disclose rich hydrogen bonding and  $\pi$ - $\pi$  stacking interactions in **1**. Interestingly, the azo additive in *o*-vanillin part is involved in fairly strong  $\pi$ - $\pi$  stacking in the solid state; therefore, such azo-aromatic group incorporation in the systems could bring interesting noncovalent interactions in the system for the stability. Regarding the catalytic oxidation of *o*-aminophenol by molecular oxygen, the compound **1** is found to be an active catalyst, while compound **2** is almost inactive, although in both cases labile positions are available at manganese centres for substrate/dioxygen binding. The structure-reactivity correlation study reveals that the stereochemical positions of labile sites in the manganese(II) center in **2** are not suitable enough for the cooperative catalytic oxidation of the substrate by molecular oxygen. These results therefore dictate that the proper stereochemical arrangements of the vacant or labile positions in the high nuclear transition metal complexes with lower oxidation state of the metal are extremely important for the cooperative catalytic activity. Such a stereochemical requisite seems not to be at all required for the metal complexes with higher oxidation state, therefore easing to develop efficient *in vitro* catalysts.

## Conflicts of interest

There are no conflicts of interest to declare.

## Acknowledgment

A.S. gratefully acknowledges the financial support of this work by the DST, India (Sanction No. SB/FT/CS-102/2014, dated- 18.07.2015). A. F. gratefully acknowledges the financial support of this work by the DGICYT of Spain (projects CTQ2014-57393-C2-1-P and CONSOLIDER INGENIO 2010 CSD2010-00065, FEDER funds). A. F. thanks the CTI (UIB) for free allocation of computer time.

## Appendix A. Supplementary data

CCDC 1478366 and 1562304 contain the supplementary crystallographic data for complexes **1** and **2**, respectively. These data can be obtained free of charge via <http://www.ccdc.cam.ac.uk/conts/retrieving.html>, or from the Cambridge Crystallographic Data Centre, 12 Union Road, Cambridge CB2 1EZ, UK; fax: (+44) 1223-336-033; or email: [deposit@ccdc.cam.ac.uk](mailto:deposit@ccdc.cam.ac.uk).

## Notes & References

<sup>a</sup>Department of Chemistry, Jadavpur University, Kolkata- 700032, India.

E-mail: [amritasahachemju@gmail.com](mailto:amritasahachemju@gmail.com); [asaha@chemistry.jdvu.ac.in](mailto:asaha@chemistry.jdvu.ac.in); Tel. +91-33-2457294.

<sup>b</sup>Departamento de Química, CICECO, Universidade de Aveiro, 3810-193 Aveiro, Portugal.

<sup>c</sup>Departament de Química, Universitat de les Illes Balears, Crta. De Valldemossa km 7.5, 07122 Palma (Balears), Spain.

E-mail: [toni.frontera@uib.es](mailto:toni.frontera@uib.es).

1 A. de Meijere, S. Bräse and M. Oestreich (Eds.), *Metal-Catalyzed Cross-Coupling Reactions and More*, Wiley-VCH Verlag GmbH & Co. KGaA, Weinheim, Germany, 2014.

2 K. Grela (Ed.), *Olefin Metathesis*, John Wiley & Sons Inc, Hoboken, NJ, USA, 2014.

3 Z. -J. Shi, *Homogeneous Catalysis for Unreactive Bond Activation*, John Wiley & Sons Inc, Hoboken, NJ, USA, 2014.

4 J. M. Thomas and W. J. Thomas, *Principles and Practice of Heterogeneous Catalysis*, Wiley-VCH Verlag GmbH & Co. KGaA, Weinheim, Germany, 2014.

5 V. P. Ananikov and M. Tanaka (Eds.), *Hydrofunctionalization*, Springer, Berlin Heidelberg, Berlin, Heidelberg, 2013.

6 D. J. Gorin, B. D. Sherry and F. D. Toste, *Chem. Rev.*, 2008, **108**, 3351–3378.

7 A. Correa, O. G. Mancheño and C. Bolm, *Chem. Soc. Rev.*, 2008, **37**, 1108–1117.

8 C. C. C. Johansson Seechurn, M. O. Kitching, T. J. Colacot and V. Snieckus, *Angew. Chem. Int. Ed.*, 2012, **51**, 5062–5085.

- 9 C. I. Ezugwu, N. A. Kabir, M. Yusubov and F. Verpoort, *Coord. Chem. Rev.*, 2016, **307**, 188-210.
- 10 I. P. Beletskaya, A. V. Cheprakov, in: T. Colacot (Ed.), *New Trends in Cross-Coupling*, Royal Society of Chemistry, Cambridge, 2014, pp. 355–478.
- 11 D. C. Powers and T. Ritter, *Acc. Chem. Res.*, 2012, **45**, 840–850.
- 12 M. García-Melchor, A. A. C. Braga, A. Lledós, G. Ujaque and F. Maseras, *Acc. Chem. Res.*, 2013, **46**, 2626–2634.
- 13 T. Sperger, I. A. Sanhueza, I. Kalvet and F. Schoenebeck, *Chem. Rev.*, 2015, **115**, 9532–9586.
- 14 J. F. Hartwig, *Organotransition Metal Chemistry: From Bonding to Catalysis*, University Science Books, Sausalito, 2010.
- 15 J. T. Groves, *J. Inorg. Biochem.*, 2006, **100**, 434–447.
- 16 B. Meunier, S. P. de Visser and S. Shaik, *Chem. Rev.*, 2004, **104** (105), 3947–3980.
- 17 P. R. Ortiz de Montellano, *Chem. Rev.*, 2010, **110**, 932–948.
- 18 W. Nam, *Acc. Chem. Res.*, 2007, **40**, 522–531.
- 19 E. I. Solomon, T. C. Brunold, M. I. Davis, J. N. Kemsley, S. K. Lee, N. Lehnert, F. Neese, A. J. Skulan, Y. S. Yang and J. Zhou, *Chem. Rev.*, 2000, **100**, 235–350.
- 20 M. Costas, M. P. Mehn, M. P. Jensen and L. Que Jr., *Chem. Rev.*, 2004, **104**, 939–986.
- 21 L. Que Jr., *Acc. Chem. Res.*, 2007, **40**, 493–500.
- 22 C. Krebs, D. G. Fujimori, C. T. Walsh and M. Bollinger Jr., *Acc. Chem. Res.*, 2007, **40**, 484–492.
- 23 A. R. McDonald and L. Que Jr., *Coord. Chem. Rev.*, 2013, **257**, 414–428; b) A. Panja, *Polyhedron*, 2014, **80**, 81–89.
- 24 E. I. Solomon, T. C. Brunold, M. I. Davis, J. N. Kemsley, S. K. Lee, N. Lehnert, F. Neese, A. J. Skulan, Y. S. Yang and J. Zhou, *Chem. Rev.*, 2000, **100**, 235–350.
- 25 E. I. Solomon, R. Sarangi, J. S. Woertink, A. J. Augustine, J. Yoon and S. Ghosh, *Acc. Chem. Res.* 2007, **40**, 581–591.
- 26 E. G. Kovaleva and J. D. Lipscomb, *Nat. Chem. Biol.*, 2008, **4**, 186–193.

- 27 E. Frei 3rd, *Cancer Chemother. Rep.*, **58** (1974) 49–54.
- 28 a) C. E. Barry III, P. G. Nayar, T. P. Begley, *Biochemistry* 1989, **28**, 6323–6333; b) C. E. Barry III, P. G. Nayar and T. P. Begley, *J. Am. Chem. Soc.* 1988, **110**, 3333–3334.
- 29 S. K. Dey and A. Mukherjee, *Coord. Chem. Rev.*, 2016, **310**, 80–115.
- 30 a) L. Fan, W. Fan, B. Li, X. Liu, X. Zhao and X. Zhang, *Dalton Trans.*, 2015, **44**, 2380–2389; b) W.H. Mahmoud, G. G. Mohamed and A.M. Refat, *Appl Organometal Chem.*, 2017, **e3753**, 1–19; c) Y. Mitsumoto, N. Sunaga and T. Akitsu, *SF J. Chem. Res.*, 2017, 1:1; d) Y. Hu, I. Sanchez-Molina, S. A. Haque and Neil Robertson, *Eur. J. Inorg. Chem.*, 2015, 5864–5873; e) M. S. Jana, A.K. Pramanik, S. Kundu, D.Sarkar, S. Jana and T. K.Mondal, *Inorganica Chimica Acta*, 2013, **394**, 583–590.
- 31 a) A. K. Dhara, U. P. Singh and K. Ghosh, *Inorg. Chem. Front.*, 2016, **3**, 1543–1558; b) M. Mitra, T. Kundu, G. Kaur, G. Sharma, A. RoyChoudhury, Y. Singh and R. Ghosh, *RSC Adv.*, 2016, **6**, 58831–58838; c) S. Sagar, S. Sengupta, A. J. Mota, S. K. Chattopadhyay, A. Espinosa Ferao, E. Riviere, W. Lewis and S. Naskar, *Dalton Trans.*, 2017, **46**, 1249–1259; d) A. Panja, M. Shyamal, A. Saha and T. K. Mandal, *Dalton Trans.*, 2014, **4**, 5443–5452; e) A. Panja, *Dalton Trans.*, 2014, **43**, 7760–7770; f) A. Panja, *RSC Adv.*, 2014, **4**, 37085–37094; g) J. Bjerre, T. H. Fenger, L. G. Marinescu and M. Bols, *Eur. J. Org. Chem.*, 2007, **2007**, 704–710; h) A. Panja and P. Guionneau, *Dalton Trans.*, 2013, **4**, 5068–5075.
- 32 M. Odabaşoğlu, Ç. Albayrak, B. Koşar and O. Büyükgüngör, *Spectrochimica Acta Part A: Molecular and Biomolecular Spectroscopy*, 2012, **92**, 357–364.
- 33 G. M. Sheldrick, *SAINTE, Version 6.02, SADABS, Version 2.03, Bruker AXS Inc.*, Madison, Wisconsin, 2002.
- 34 G. M. Sheldrick, *SADABS: Software for Empirical Absorption Correction*, University of Göttingen, Institute für Anorganische Chemie der Universität, Göttingen, Germany, 1999–2003.
- 35 G. M. Sheldrick, *SHELXL-2017/1, Program for the Solution of Crystal Structures*, University of Göttingen, Germany, 2017; b) G. M. Sheldrick, *Acta Crystallogr.*, 2015, **C71**, 3–8.
- 36 R. Ahlrichs, M. Bär, M. Häser, H. Horn and C. Kölmel, *Chem. Phys. Lett.*, 1989, **162**, 165–169.

- 37 A. Bauzá, A. Terrón, M. Barceló-Oliver, A. García-Raso and A. Frontera, *Inorg. Chim. Acta.*, 2016, **452**, 244–250; b) D. Sadhukhan, M. Maiti, G. Pilet, A. Bauzá, A. Frontera and S. Mitra, *Eur. J. Inorg. Chem.*, 2015, **11**, 1958–1972; c) M. Mirzaei, H. Eshtiagh-Hosseini, Z. Bolouri, Z. Rahmati, A. Esmailzadeh, A. Hassanpoor, A. Bauza, P. Ballester, M. Barceló-Oliver, J. T. Mague, B. Notash and A. Frontera, *Cryst. Growth Des.*, 2015, **15**, 1351–1361; d) P. Chakraborty, S. Purkait, S. Mondal, A. Bauzá, A. Frontera, C. Massera and D. Das, *CrystEngComm*, 2015, **17**, 4680–4690.
- 38 S. F. Boys and F. Bernardi, *Mol. Phys.*, 1970, **19**, 553–555.
- 39 K. Nakamoto. *Infrared and Raman Spectra of Inorganic and Coordination Compounds*, Part B, 6th Edn., John Wiley & Sons, New Jersey (2009).
- 40 a) A. Panja, N. Shaikh, M. Ali, P. Vojtíšek, P. Banerjee, *Polyhedron*, 2003, **22**, 1191–1198; b) S. Naskar, S. Naskar, R. J. Butcher, M. Corbella, A. Espinosa Ferao, and S. Kumar Chattopadhyay, *Eur. J. Inorg. Chem.*, 2013, 3249–3260.
- 41 A. W. Addison, T. N. Rao, J. Reedjik, J. V. Rij and C. G. Verschoor, *J. Chem. Soc., Dalton Trans.*, **1984**, 1349–1356.
- 42 a) S. Banerjee and A. Saha, *Journal of Coordination Chemistry*, 2016, **69(20)**, 3092–3106; b) A. Panja, *Polyhedron*, 2014, **79**, 258–268.
- 43 L. Ruhlmann, A. Nakamura, J. G. Vos, and J. -H. Fuhrhop, *Inorg. Chem.*, **37**, 1998, 6052–6059.
- 44 N. C. Jana, P. Brandão and A. Panja, *J. Inorg. Biochem.*, 2016, **159**, 96–106.

## Table of Contents Entry

# Nuclearity versus oxidation state in catalytic efficiency of Mn<sup>II/III</sup> azo Schiff base complexes: Computational study on supramolecular interactions and phenoxazinone synthase like activity

Saikat Banerjee,<sup>a</sup> Paula Brandão,<sup>b</sup> Antonio Bauzá,<sup>c</sup> Antonio Frontera,<sup>\*c</sup> Miquel Barceló-Oliver<sup>c</sup>, Anangamohan Panja,<sup>d</sup> and Amrita Saha,<sup>\*a</sup>

<sup>a</sup> Department of Chemistry, Jadavpur University, Kolkata- 700032, India.

E-mail: amritasahachemju@gmail.com; asaha@chemistry.jdvu.ac.in; Tel. +91-33-2457294.

<sup>b</sup> Departamento de Química, CICECO, Universidade de Aveiro, 3810-193 Aveiro, Portugal.

<sup>c</sup> Departament de Química, Universitat de les Illes Balears, Crta. De Valldemossa km 7.5, 07122 Palma (Balears), Spain.

E-mail: toni.frontera@uib.es.

<sup>d</sup> Postgraduate Department of Chemistry, Panskura Banamali College, Panskura RS, WB 721152, India.

